Influence of miR-155 on Murine ATII Cell Gene Expression during Influenza Infection

Undergraduate Research Written Thesis

Presented in Partial Fulfillment of the Requirements for graduation "with Honors Research Distinction in Microbiology" in the undergraduate colleges of

The Ohio State University

Adam Bercz

The Ohio State University

April 2018

Project Advisor: Ian Davis, DVM/PhD, Department of Veterinary Biosciences

Committee Members

Natacha Ruiz, PhD

Chad Rappleye, PhD

Ian Davis, DVM/PhD

Table of Contents

I. Abstract

Influenza has an extensive history of crippling global populations and remains prevalent due to a high mutation rate. This feature of influenza explains why new vaccines are developed and administered annually, yet no effective treatment for severe cases exist. Previous findings have shown an increase of certain microRNAs (miRs*)* in response to influenza infection. Examining the role of these molecules, specifically miR-155, may reveal critical knowledge on disease development. This small nucleic acid's expression increases consistently over a 6-day course of influenza infection in a murine model (C57BL/6). This leads us to believe that miR-155 plays an important role in the inflammatory response to influenza infection, leading to acute respiratory distress syndrome (ARDS), a condition of major clinical relevance.

Alveolar type 2 (ATII) cells are a key cell type in the distal lung and are also a primary target for influenza A viruses. Infected and non-infected population of these cells can be isolated by utilizing a genetically engineered fluorescent virus and flow-sorting based on fluorescence. Subsequent real-time PCR allows for quantification of miR-155 and its target genes. miR-155 levels are higher in mCherry-positive ATII cells compared to mCherry-negative cells from mice infected with fluorescent PR8-mCherry influenza virus. Target genes of miR-155, including antiviral factors and regulators of cytokine production, have been shown to differ in expression between virally infected and uninfected populations ATII cells of the same mouse.

The information drawn from this project may lead to identification of new targets for therapeutic agents which enhance the host's immune capability to fight off newly emerging strains of influenza.

II. Introduction:

A. Historical Background

Influenza is a human pathogen with a deep-rooted history in public health. While influenza was first described in the 16th century, the most notable outbreak of the viral disease occurred in 1918. Contrary to its name “Spanish influenza”, the outbreak did not localize itself to Spain but reached pandemic proportions of transmission and spread. The 1918 pandemic remains one of the most fatal biological events in entire human history, comparable to the bubonic plague. It is estimated that more than 50 million people died globally[1]. Although unknown at the time, the influenza virus cross over from avian reservoirs and is therefore considered a major zoonotic disease today[2].

B. Influenza A Virus

The type A and B subsets of influenza is responsible for annual strains of influenza which affect human and animal populations. Influenza A virus (IAV) is a negative sense, segmented, single stranded RNA virus belonging to the orthomyxoviridae family. The segmented nature of influenza virus allows for genes segments to be exchanged between another different virions within the same host cell[3]. Subsequent shifts in the hemagglutinin and neuraminidase glycoproteins of the viral surface result in novel antigens, meaning that the host immune cells will not recognize the virus upon exposure. The consequence of this process of antigenic shift is that preventative measures against the virus, such as vaccination, are insufficient in producing long term immunity due to the seasonal variability in viral strains. Antigenic

drift, or the gradual changes in genetic sequence of the virus, also contribute to difficulties in managing public health responses to influenza strains.

C. Alveolar Type II Cells

Alveolar type II (ATII) cells are one of two epithelial cell types that line the alveolar surface. Although ATII cells only make up roughly 5% of the surface, they account for about 50% of total cells. ATII cells have major roles pulmonary function. Key functions of this cell type include vectorial ion transport, differentiation in ATI cells during lung repair after injury, regulation of monocyte transfer across epithelium, and the secretion of lung surfactant lipid and proteins[4,5].

Not only do ATII cells perform critical functions for maintaining lung homeostasis, but they are also a primary site of IAV replication in individuals with severe lower respiratory tract disease[6] and contribute to the innate immune response to this pathogen.

D. MicroRNA

MicroRNAs span from 21-25 nucleotides in length and contribute to a dynamic range of regulatory functions in biological systems[7], by exerting effects on transcriptomics by binding specific mRNA consensus sequences to degrade the nucleic acid or repress translation[8].

Specifically of interest in regards to influenza infection is the expression of microRNA-155 (miR-155) and the regulatory role it plays in the ATII cellular response of influenza infection. miR-155 has been shown to play an important role in the pro-inflammatory response of respiratory epithelial cells to a variety of insults[10]. In preliminary studies conducted by the Davis lab, it was reported that miR-155 expression is

progressively up-regulated over the course of 6 days in ATII cells from mice infected with influenza A/WSN/33 (H1N1) IAV. However, not all these ATII cells contain replicating virus. This observation led to the hypothesis that miR-155 expression profiles will differ between ATII cells containing replicating virus, and those which do not contain non-replicating virus. miR-155 expression is likely not homogeneous within a population of isolated ATII cells, making it important to develop a model for distinguishing infected versus non-infected cells.

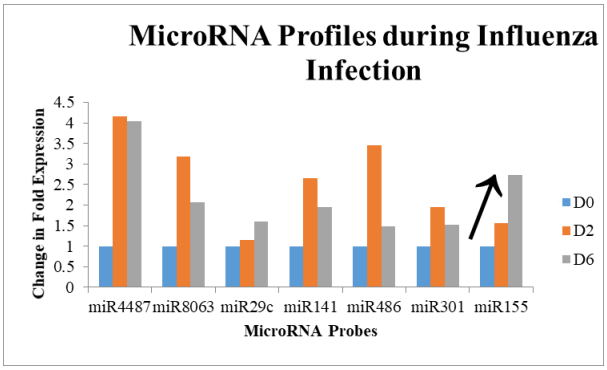

Figure 4: RT-PCR probes measured changes in microRNA expression in ATII cells at 2 and 6 days post infection with WSN influenza A virus

E. Project Overview

Since microRNAs have been shown to exert a broad regulatory effect on the expression of genes in an *in vivo* model, it follows that there may be observable changes in regulation in response to influenza infection. We aimed not only to characterize how IAV alters the dynamics of a whole-lung in a WT and miR-155 knockout model, but also how miR-155 expression differs from ATII cells containing replicating virus and ATII cells not containing replicating virus. Consequently, we aimed to assess how miR-155 targets genes are expressed in these different cellular phenotypes. The knowledge of the impact of miR-155 at the cellular level may help lead to identification of potential targets for host-directed therapeutics against influenza infection.

III. Materials and Methods

A. Mouse Model and Infection

Wild-type (WT) C57BL/6 mice were obtained from Charles River Laboratories between eight and twelve weeks of age. After sedation using a mixture of ketamine and xylazine, mice were inoculated with 50,000 plaque-forming units (PFU) of PR8/mCherry/NS1 (H1N1) virus[9]. Control mice were mock-infected with the inoculum virus diluent (0.1% BSA in PBS). The 50 μL inoculum was administered intranasally over the course of 5-10 minutes. Genetically engineered through a ATII cell-specific cre-lox system, a strain of C57BL/6 miR-155 knockout (miR-155 KO) mice were also used in this study.

B. Mouse Monitoring

Mock-infected and infected mice were closely monitored for the duration of the experiment, either 2, 4, or 6 days. Pulse Oximeter and body weight measurements were performed every other day throughout the experiments.

C. ATII Cell Isolation

Alveolar type II cells were isolated at either 2, 4, or 6 days post-infection (dpi). The lungs were perfused with heparin solution, before being placed in suspension for dispase and DNAase digestion[10]. Filtrations were performed using 100 and 25um nylon meshes to obtain a single cell suspension. Cell counts were performed and viability assessed via trypan blue staining. Based on these cell counts, appropriate quantities of biotinylated antibodies against CD45, CD16/32, CD31, CD104, and TER119 were added to each sample. Following a 20-minute incubation, streptavidin beads were

added to bind the antibodies and cells were incubated for an additional 20 minutes on ice. The cell suspensions were sorted through automacs magnetic columns, to isolate populations of alveolar type II cells by negative selection. Purity of isolated ATII cells were confirmed by flow cytometry.

D. Aria III Flow Sorting

Isolated alveolar type II cells were sorted by flow cytometry based on mCherry fluorescence using a 561 nm laser of an Aria III instrument (OSUCCC Analytical Cytometry Core). Based on gating against a mock-infected pool of isolated cells, cells expressing mCherry fluorescence were isolated in addition to cells not expressing fluorescence within the same murine lung. Total cell counts and percentage of each population were obtained, respective to total ATII cells isolated.

E. PCR Array Analysis of Genes Associated with miR-155

Total RNA of ATII cells was isolated using TRIzol reagent(Invitrogen: Carlsbad, California) and purified using a miRNeasy kit (Qiagen: Hilden, Germany). Quantification of the RNA was performed using a Nanodrop ND-1000 spectrophotometer (ThermoScientific: Carlsbad, California). For PCR array analysis >100ng of total RNA was reverse transcribed to cDNA using the RT^2 First Strand kit as per manufacturer's instructions (Sabbiosciences: Frederick, Maryland). The cDNA was preamplified using a miR-155 pathway primer mix (Qiagen: Hilden, Germany) and added to miR-155 target array plates(PAMM-6002ZC-12) in 25 μL volumes. To normalize data from the PCR arrays, cycle threshold (CT) values of target genes were measured against the average CT values of the housekeeping genes β-actin, β-2 microglobulin, glyceraldehyde 3

phosphate dehydrogenase, β-glucuronidase, and α-heat shock protein 90. This method allowed for comparing relative gene expression among experimental groups, including ATII cells positive for mCherry protein, ATII cells negative for mCherry protein, and mock-infected cells. The differences between groups is represented by fold-change on Log_2 scale.

F. Quantitative Real-Time PCR

To measure expression of mRNA for additional target genes, total RNA was reverse-transcribed into cDNA using a High Capacity cDNA Reverse Transcription Kit (Applied Biosystems). Real-time quantitative PCR (Qpcr) experiments were performed by adding >6 ng of cDNA to murine specific gene probes (Life Technologies: Carlsbad, California). Gene expression CT values were normalized with respect to the 18s rRNA housekeeping gene.

G. Immunofluorescence and Confocal Microscopy

To confirm the expression patterns obtained from real-time data, immunofluorescent staining was performed. ATII Cells were initially fixed in formalin and observed using confocal microscopy following primary antibody incubation against interferon gamma receptor (IFNγr) and nuclear staining with DAPI.

H. In Vivo Imaging System

An *In Vivo* Imaging System was used to assess the intensity of red fluorescence protein in extracted whole lungs of mice at 0, 2, 4 and 6 days post infection.

IV. Results

50,000 PFU is the dose sufficient to induce Acute Respiratory Distress (ARDS) at 6-days post-PR8mCherry infection

The PR8/mCherry/NS1 virus serves as a fluorescent tool which allows for differentiation between ATII cells that do and do not contain actively replicating virus. However, there was no previously established knowledge on viral dosage sufficient to induce clinical signs consistent with ARDS. A dose-response experiment was performed to determine the optimal concentration of PR8/mCherry/NS1 virus to use for intranasal infection. Previous studies have determined the LD_{50} of the PR8/mCherry/NSI virus in C57/B6 mice however the endpoint in this project was development of ARDS clinical signs[11]. The clinical signs of ARDS in mice include consistent with hypoxemia, significant loss in body weight, increased water content in lungs, and reduced lung compliance[12].

Figure 5 Changes in health parameters associated with ARDS

A) The amount of fluid build-up in murine lungs were measured by at 6dpi at various viral doses **B)** Changes in murine body weight were recorded over a course of 6 days following infection in response to the viral doses administered **C)** The levels of oxygen saturation in murine lungs were measured over the course of influenza infection **D)** Comparison of a healthy (left) and PR8/mCherry virally

A

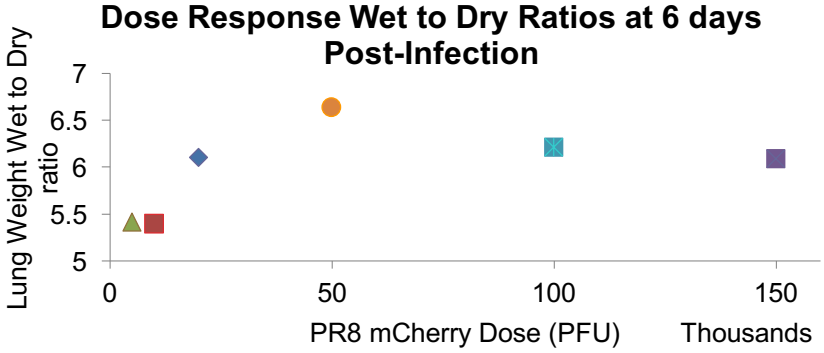

B

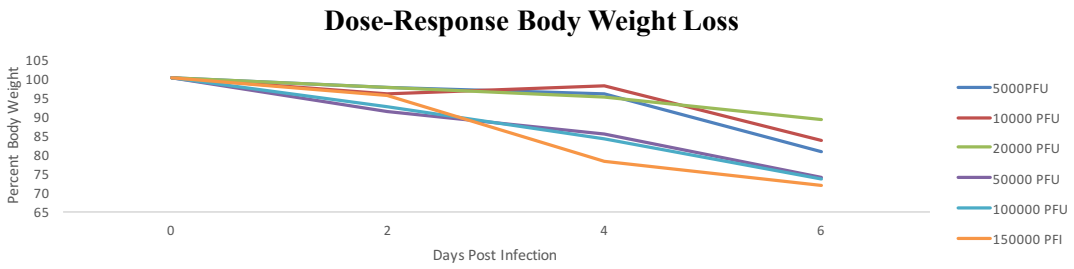

C

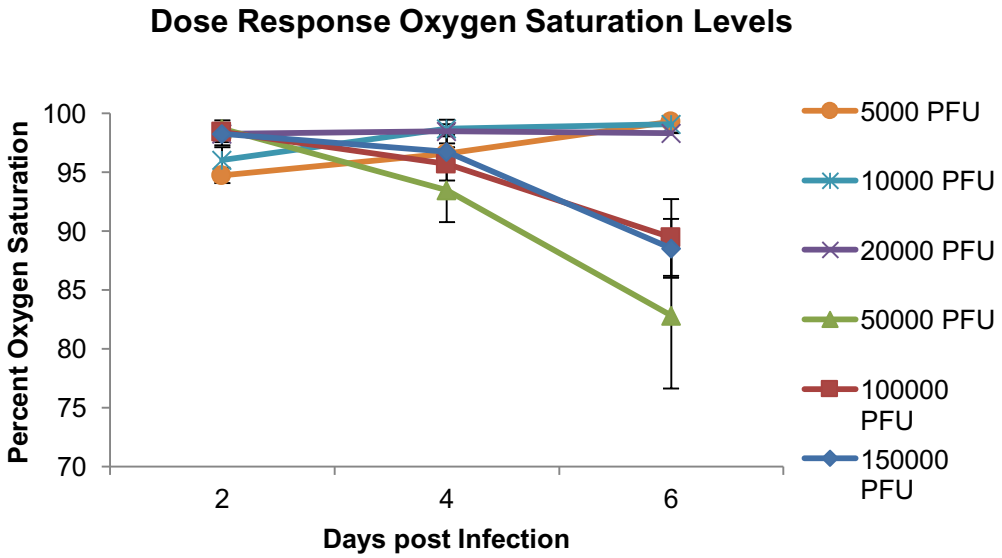

D

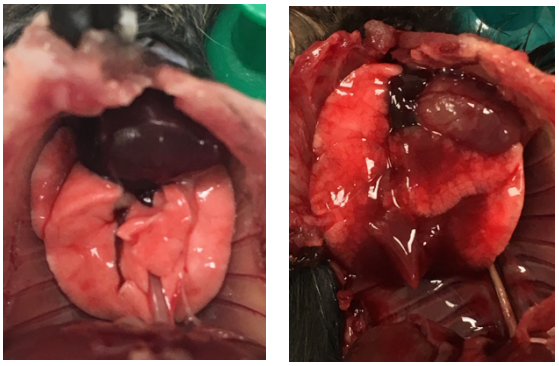

While higher doses were tested, oxygen saturation was most depressed in mice infected with the 50,000 PFU dose. This dose also affected body weight similarly to doses containing double and triple the amount of PFUs. Therefore, intranasal infection with a 50,000 PFU dose of PR8/mCherry/NS1 virus resulted in development of lung

dysfunction most consistent with an onset of ARDS. The 50,000 PFU dose was used in all proceeding experiments.

Whole lungs of C57/B6 mice contain a large viral burden at 4 and 6 days post-infection

With the establishment of a viral dose, the next experimental parameter to determine was the most appropriate time-point for ATII cell isolation and gene-expression studies. Assessment of viral burden at various time-points was performed to determine optimal time-points for isolating ATII cells. IVIS imaging revealed the intensity of red fluorescent proteins in whole lungs isolated at 6 dpi, 4 dpi, 2 dpi, and in a mock-infected control lung. The peak fluorescence was measured from whole lung isolated at 4 dpi. Although the peak fluorescence indicates the greatest viral burden, clinical signs are not most severe at 4 dpi but rather 6 dpi. This finding suggest that severe changes in the overall health of an *in vivo* model is not due to the influenza pathogen itself, but the changes in tissue integrity and immune function which result from the viral presence. Therefore, the 4 dpi time-point was selected to investigate changes the infection status and changes in gene expression in ATII cells that may contribute to the broader self-damaging host response.

Figure 6 Fluorscence of the mCherry protein is highest at 4 dpi (right): Imaging of murine lungs *ex-vivo* showed that viral burden in the lung differed through the course of influenza infection

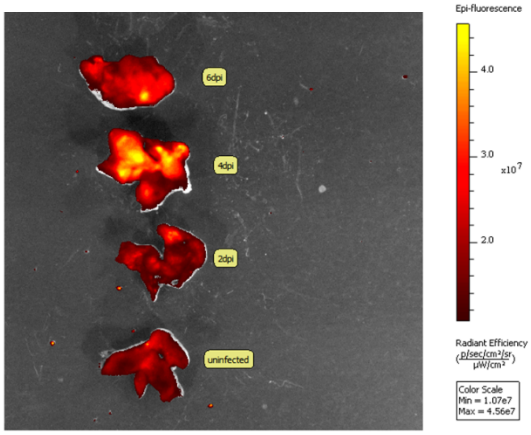

ATII isolation and characterization of subpopulations based on mCherry Status

Isolation of ATII cells at 4dpi resulted in consistent collection of >10^6 cells per lung, which maintained a viability of at least 70%. The purity of ATII isolation was confirmed by flow cytometry, as the isolated population of cells consistently contained >90% $CD45^-$ cells, which is a marker used to negatively select for ATII cells. The isolated ATII populations were further sub-divided via flow-sorting. ATII cells were categorized as virus-positive or virus-negative based on the presence or absence of mCherry fluorescence.

Figure 7 Isolation of ATII cells resulted in pure populations subdivided into $mCherry^+$ and $mCherry^-$ groups: A) Flow panel shows crude cell populations (red) and pure ATII populations (black) **B)** Flow panel shows selective gating of whole ATII cell population into red fluorescent protein (RFP) positive or negative clusters **C)** Yields of RFP-containing ATII cells were slightly higher in ATII population unable to express miR-155

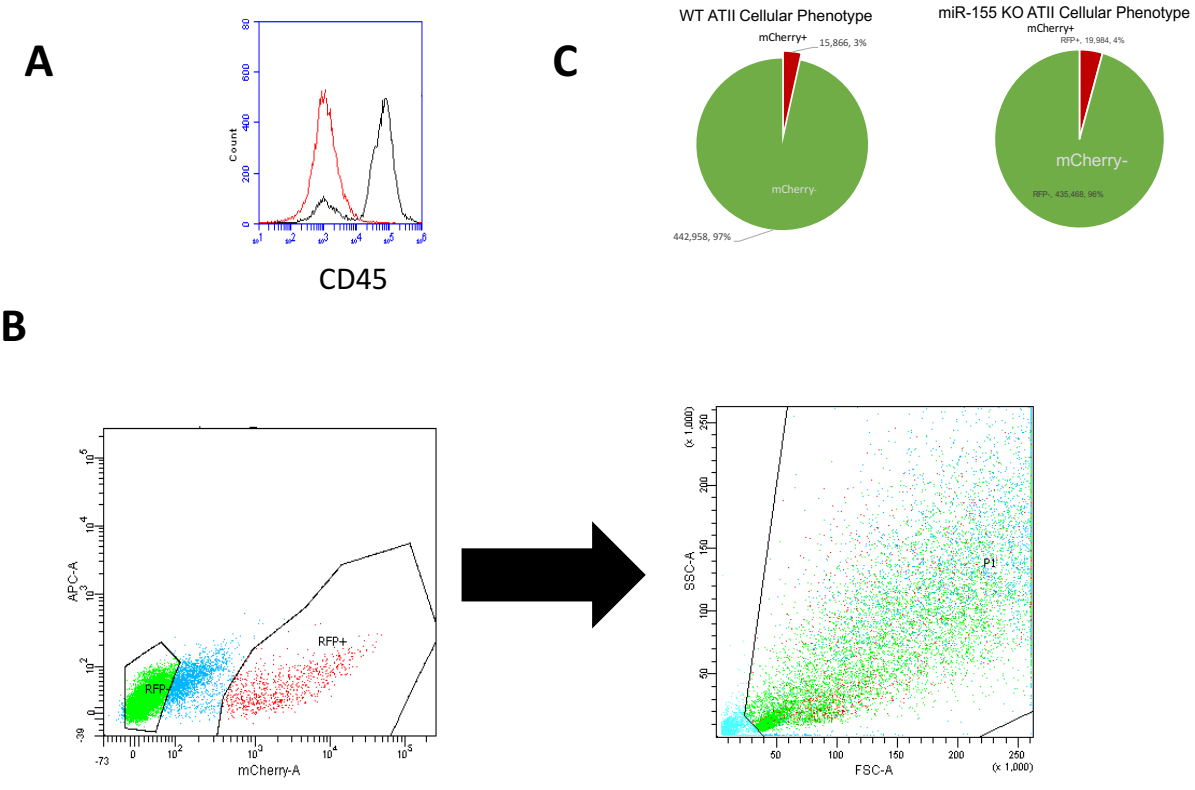

miR-155 is expressed at a higher level in flow-sorted mCherry^{+} ATII Cells than mCherry^{-} and mock-infected ATII cells

Relative to ATII cells that did not contain mCherry protein from an infected lung and mock-infected populations, mCherry^{+} cells expressed the greatest amount of miR-155. Normalization was performed relative to the endogenous control gene *sno202.*

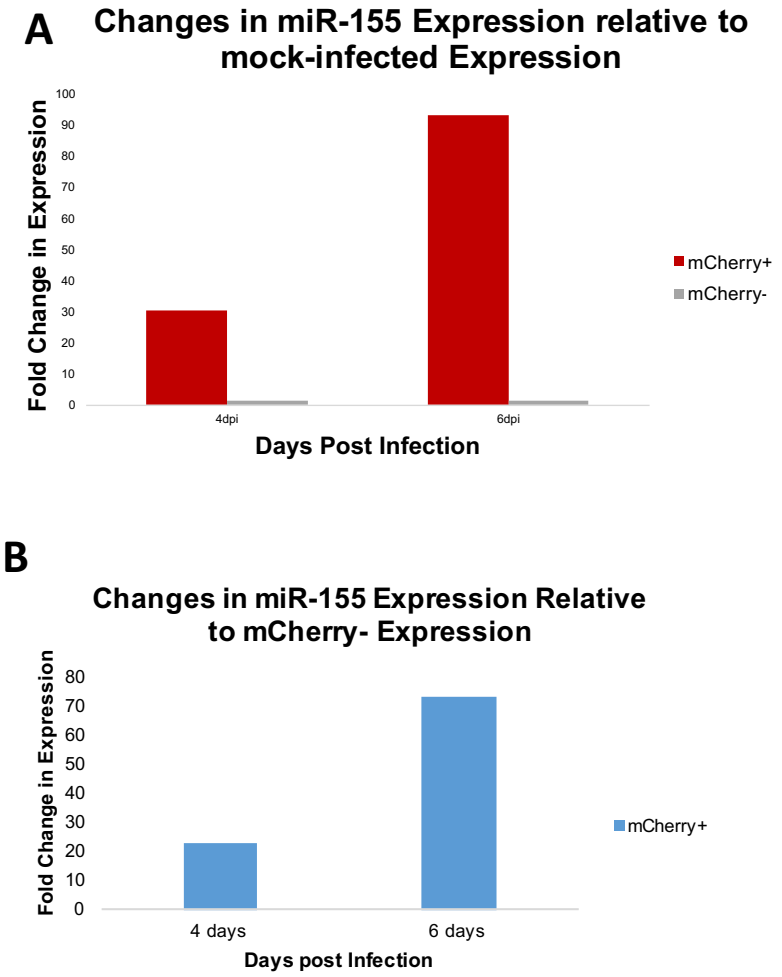

Figure 8 (left) Mir-155 expression is differs depending on mCherry presence in ATII cells A Fold change in expression of miR-155 was compared in mCherry^{+} and mCherry^{-} ATII cells relative to a mock-infected control at 4 and 6 dpi. **B** Relative to mCherry^{-} ATII cells, cold

Upregulation of miR-155 is correlated with a robust downregulation of miR-155 target genes in miR-155 expressing mCherry^{-} ATII cells

Analysis of messenger-RNA levels in wild-type ATII cells revealed differing profiles of miR-155 target gene expression. Between mCherry^{+} and mCherry^{-} ATII cells, the higher miR-155 levels in mCherry^{+} contributed to heterogeneous regulation of gene products, whereas the lower levels of miR-155 in mCherry^{-} cells correlated to downregulation in most of the target genes.

<u>Figure 9 (below)</u> Known target genes of miR-155 are differentially expressed within ATII cells of the same infected lung A) Heat-maps were generated showing differences in mRNA levels of miR-155 target genes from WT ATII cells **B)** List of the identities, location on heat map, functions, and change in regulation of the differentially regulated miR-155 target genes

A

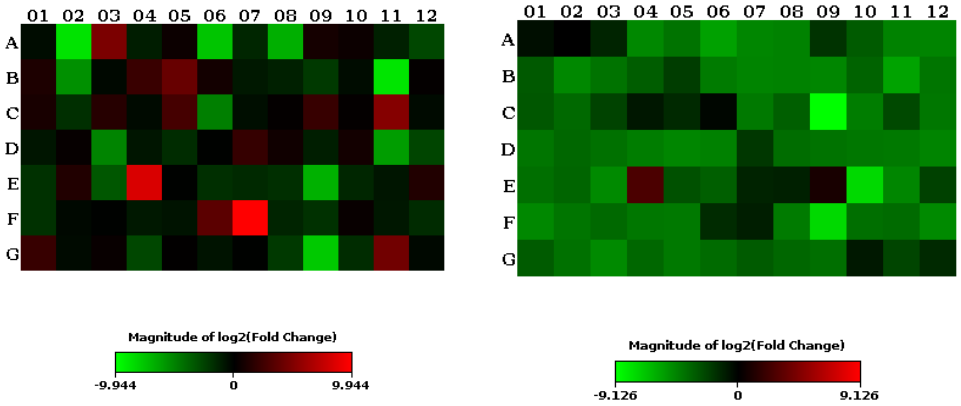

B

Gene	Function	Expression relative to WT mock
Angiotensin receptor 1a (Agtr1a)- A02	Regulates sodium-potassium ATPase, as well as blood pressure and fluid balance	Decreased in mCherry^{+} cells, no difference in mCherry^{-}
Interleukin-1 receptor associated kinase 3 (Irak3)- C06	Negative regulator of TLR system	decreased in mCherry^{+} cells, no difference in mCherry^{-}

SRY-Box 1 (Sox1)- F07	Transcriptional activator for RNA polymerase II	Increased in mCherry^{+} cells, decreased in mCherry^{-}
Activation induced cytidine deaminase(Aicda)- B03	Critical in B-cell developmental process of somatic hypermutation, gene conversion, and class-switching	Increased in mCherry^{+} cells, decreased in mCherry^{-}
MAF BZIP transcription factor B (Mafb)- C11	Represses ETS-1 to regulate hematopoesis	Increased in mCherry^{+} cells, decreased in mCherry^{-}
Runt related transcription factor 2 (Runx2)- E09	Regulator in skeletal development and linked to fibrosis of lung tissue	Decreased in mCherry^{+} cells, no difference in mCherry^{-}
Endothelin 1 (Edn1)- B05	Potent vasoconstrictor	Increased in mCherry^{+} cells, decreased in mCherry^{-}

There is no significant change in mRNA levels between mock infected WT ATII cells and ATII cells with the miR-155 locus knock-out

To assess if wild-type ATII cells express miR-155 target genes differently than the ATII cells lacking miR-155 expression, the mRNA levels of miR-155 targets were compared in mock-infected populations of the two phenotypes.

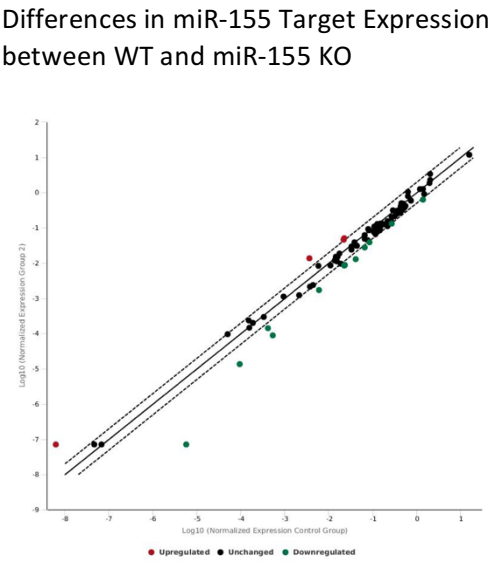

Figure 10 (left) miR-155 has minimal influence on target gene expression in ATII cells of non-infected lungs Few miR-155 target genes were differentially regulated when comparing WT and miR-155 KO ATII cells

Isolated from ATII-specific miR-155 KO mice, miR-155 target mRNA levels are heterogeneously expressed between mCherry^{+} and mCherry^{-} ATII cells

Analysis of messenger-RNA levels in miR-155 ATII cells revealed similar profiles of miR-155 target gene expression. The absence of miR-155 expression contributed to up and down-regulation of targets genes in both mCherry^{+} and mCherry^{-} ATII cells. The magnitude of target gene expression was lower in mCherry^{-} ATII cells compared to the mCherry^{+} population.

Figure 11 (below) Known target genes of miR-155 are expressed heterogeneously in both A) Heat-maps were generated showing the differences in mRNA levels of miR-155 target genes in miR-155 KO ATII celles **B)** List of the identities, location on heat map, functions, and change in regulation of the differentially regulated miR-155 target genes

A

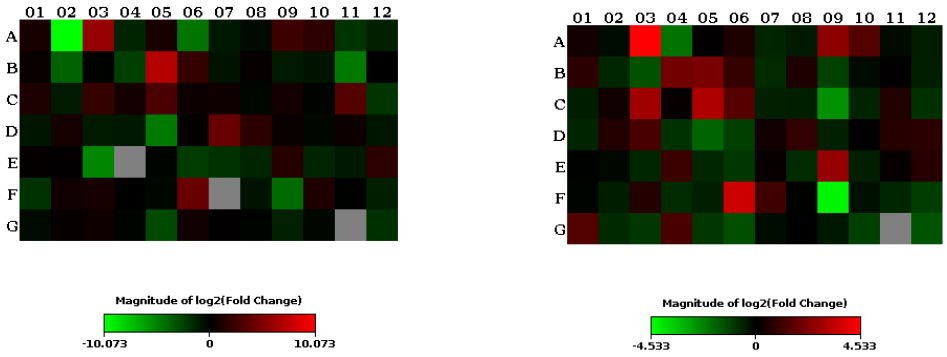

B

Gene	Function	Expression relative to KO mock
Angiotensin receptor 1a (Aggtr1a)- A02	Regulates sodium-potassium ATPase, as well as blood pressure and fluid balance	Decreased in $mCherry^+$ cells, no difference in $mCherry^-$
Caspasse recruitment domain family 11 (Card11)- A09	Acttivates NF-kB, stimulation of T-cells and positively regulates apoptosis	decreased in $mCherry^+$ cells, decreased in $mCherry^-$
Dynein cytoplasmic 1 intermediate chain 1 (Dync1i1)- B04	Factor in dynein cytoplasmic complex responsible for intracellular motility of organelles and vesicles along microtubules	decreased in $mCherry^+$ cells, increased in $mCherry^-$
Leucine zipper down-regulated in cancer 1 (Ldoc1)- C09	Inhibits activation of NF-kappaB	No difference in $mCherry^+$ cells, decreased in $mCherry^-$
Meis Homeobox 1 (Meis1)- D03	Transcriptional activator of PF4, a CXC chemokine	decreased in $mCherry^+$ cells, increased in $mCherry^-$

V. Discussion

Studying the dynamics of the host-response to influenza is an important component of managing infectious disease. Current treatment options for influenza patients are limited, especially in cases of ARDS, and current antivirals largely serve to alleviate symptoms and not treat the disease.

Since microRNAs act globally on regulating gene expression in eukaryotic cells, it is thought that they also play an important role in responding to pathogens. A hallmark feature of influenza pathology is the “cytokine storm” that occurs in the host in response to influenza replication[13]. miR-155 has been shown to play a role in regulating the expression of pre-inflammatory genes, so studying its role in an important cell type implicated during influenza infection may provide key insights to better management of the disease before severe clinical signs develop.

This study found that mRNA of miR-155 targets are differentially expressed between ATII cells that contain replicating virus and do not contain replicating virus.

Relative to mock-infected mice, miR-155 targets show a nearly global downregulation in $mCherry^-$ cells isolated from wild-type mice. Although the levels of miR-155 are lower in $mCherry^-$ cells than $mCherry^+$, its role appears to be more profound in virus-negative cells. This was shown by the robust downregulation of 78 of the 84 miR-155 targets investigated. The regulatory effect of miR-155 in infected WT ATII cells did not differ greatly compared to infected miR-155 KO ATII cells. This finding suggests that the influenza virus suppresses the function of miR-155 at an intracellular level. However, there were four targets that showed differential expression in infected

WT ATII cells and were therefore regulated independently of influenza prescence. These targets were Irak3, Bcorl1, Runx2, and Zfp407. The role of Irak3 is linked to negative regulation of toll-like receptor signaling system[14], so its downregulation may contribute to the pro-inflammatory microenvironment which occurs during influenza infection. Runx2 transcripts have been shown to be upregulated within ATII cells in clinical human cases of pulmonary fibrosis[15], however with the 4dpi timepoint used in this experiment, such lung pathology was not evident and interestingly, Runx2 transcripts were downregulated in both $mCherry^+$ and $mCherry^-$ cells. Further investigations on Runx2 expression at 6dpi, when lung pathology is greater than 4dpi, may reveal differences in gene expression that occur independently of miR-155 regulation. The consequences of miR-155 dependent downregulation of Bcorl1 and Zfp407 in response to influenza infection are not clear.

While differences exist in miR-155 target gene expression between infected WT and miR-155 KO ATII cells, it is important to note that only 3% of ATII cells from infected lungs contained actively replicated PR8/mCherry/NS1 virus. Therefore, the important effects of flu infection on the microenvironment in the distal lung may be more significant than the impact of actively infected cells alone. Although $mCherry^-$ ATII cells express less miR-155 than neighboring $mCherry^+$ cells, it appears that the lack of virus allows miR-155 to regulate target genes more efficently than in virus-detected cells.

The increased expression of miR-155 in $mCherry^+$ WT ATII cells may be partially due to the increased expression of Sox1, which is a known RNA polymerase II activator. RNA polymerase II is the enzyme in eukaryotic cells which is responsible for transcription of micro and small non-coding RNAs, including miR-155[16]. This finding

suggests that a positive-feedback mechanism contributes to the high expression of miR-155 in mCherry^{+} cells, while miR-155 levels are lower in mCherry^{-} cells which also display no difference in Sox1 mRNA expression compared to mock-infected ATII cells. MafB upregulation was observed in WT ATII cells containing virus, a factor known to interact with and repress the Ets1 transcription factor which is key in coordinating cytokine expression in immune cell activation[17].

The absense of miR-155 expression led to differential target gene expression in an ATII-specific miR-155 knockout model. The nearly global downregulation of miR-155 targets in WT mCherry^{-} ATII cells was not observed in the same population of the knockout model. However, the regulation of certain targets suggests that the regulation of miR-155 targets leads to inflammatory response that differs from that observed in the WT model. In mCherry^{-} cells unable to express miR-155, Ldoc1 is downregulated while Card11 is upregulated. Both of these genes acts on the NF-kB pathway, an important immune cascade in respondingto pathogens. Ldoc1 inhibits the activation of the NF-kB transcription factor[18] while Card11 activates it[19], so the observed levels of expression indicate that the abundant virus-negative population is amplifying the NF-kB pathway in response to local virally infected cells. Furthermore, both Card11 and Ldoc1 positively regulate apoptosis, suggesting that induced cell death is being antagonistically regullted. However, Runx2 in this abundant virus-negative phenotype is higher than the locally infected cells, suggesting that there may be a greater risk of fibrosis development in the miR-155 knockout model. The level of regulation of these genes is unchanged in mCherry^{+} cells compared to a mock-infected population of ATII cells.

As miR-155 expression is greatest in mCherry$^+$ cells, the difference of gene expression between WT and miR-155 KO ATII cells may provide insights on the interactions between influenza A virus and miR-155. The decreased levels of Irak3 transcripts in the WT population of mCherry$^+$ promotes the TLR signaling and in turn, activates the innate immune response. An overly activated innate immune response contributes damaging lung tissue that is often seen in cases of severe influenza disease. However, Runx2 is lower in the WT population which suggests that at 4dpi, pulmonary fibrosis may be less likely to development in contrast to the miR-155 KO ATII population. Increased Dync1i1 transcripts correlate to increased membrane traffic[20] in the WT population, which suggests a change in cellular activity in response to the influenza pathogen. Lastly, in both groups of mCherry$^+$ ATII cells, the level of Angtr1a transcripts was downregulated . As a part of the renin-angiotensin system, this downregulated receptor could be contributing to vasodilation and suppressed aldosterone levels, which are responses that lead to infiltration of inflammatory markers in local tissue[21]. Influenza A virus acts to block the effects of the angiotensin receptor regardless of miR-155 expression.

Future directions for this study include the validation of transcriptomic data via phenotyping experiments and transitioning into the investigation of changes to miR-155 regulation at 6dpi. For example, the level of Runx2 expression at 6dpi may serve as a better indicator of pulmonary fibrosis development than the levels at 4dpi, when severe lung pathology is not evident in a mouse model. In addition, the lung compliances will be measured between the two strains of mice utliized in this study in order to assess differences in clinical sign development. Analysis of bronchoaleveolar fluids from both

strains will also provide insights to whether differences in miR-155 expression in the alveolar space influence the environment of infected whole lungs. Conducting these studies will hopefully illuminate potential therapeutic options that alleviate the role of miR-155 in the inflammatory cascade that leads to cases of influenza disease. Additonally, this potential host-focused therapeutic could serve as an alternative that provide a treatment option independent of viral strain and disease severity.

VI. Acknowledgements

Special thanks to the Department of Veterinary Biosciences for their support and constructive feedback on my progress during joint-lab meetings. Thank you to the Department of Microbiology and the following sponsors of my undergraduate research:

- ATS Foundation Recognition Award for Outstanding Established Investigators (Davis)
- Research Scholar Award (Bercz)
- URO Undergraduate Summer Fellowship (Bercz)
- SOLAR Award (Bercz)
- 2016 Undergraduate Research Scholarship (Bercz)
- 2017 Undergraduate Research Scholarship (Bercz)

Countless thanks go to the entire Davis Lab for their professional mentorship, dedication to scientific training, and intangible benefits I have gained from the personal relationships. Each of the lab members listed below provided support in a variety of ways, and without such guidance, completing a rigorous undergraduate thesis project would have been far more difficult and I would not be near the scientist I am today.

- Ian Davis, DVM/PhD
- Lauren Doolittle, PhD Candidate
- Lucia Rosas, DVM
- Lisa Joseph, RVT
- Parker Woods, PhD
- Nicholas Ursini, PhD student

Thank you to my parents for their unconditional support and wisdom. They are the support system that inspired me to pursue my goals and maintain positivity throughout, even through setbacks.

And lastly, I owe my passion for science to my grandfather, Jeno Peter Bercz, whose dedication to environmental protection research inspired me from a young age. Every day, I strive to model myself on his merits and live up to the legacy he left behind.

VII. References

1. Taubenberger, J. K., & Morens, D. M. (2008). The pathology of influenza virus infections. *Annual Review of Pathology*, *3*, 499–522. https://doi.org/10.1146/annurev.pathmechdis.3.121806.154316
2. Ma, W., Kahn, R. E., & Richt, J. A. (2009). The pig as a mixing vessel for influenza viruses: Human and veterinary implications. *Journal of Molecular and Genetic Medicine*, *3*(1), 158–166. https://doi.org/10.4172/1747-0862.1000028
3. Boivin, S., Cusack, S., Ruigrok, R. W. H., & Hart, D. J. (2010). Influenza A virus polymerase: Structural insights into replication and host adaptation mechanisms. *Journal of Biological Chemistry*, *285*(37), 28411–28417. https://doi.org/10.1074/jbc.R110.117531
4. Stegemann-Koniszewski, S., Jeron, A., Gereke, M., Geffers, R., Kröger, A., & Gunzer, M. (2016). Alveolar Type II Epithelial Cells Contribute to the Anti-Influenza A Virus Response in the Lung by Integrating Pathogen- and Microenvironment-Derived Signals. *mBio*, *7*(3), 1–11. https://doi.org/10.1128/mBio.00276-16.Editor
5. Andreeva, A. V., Kutuzov, M. A., & Voyno-Yasenetskaya, T. A. (2007). Regulation of surfactant secretion in alveolar type II cells. *AJP: Lung Cellular and Molecular Physiology*, *293*(2), L259–L271. https://doi.org/10.1152/ajplung.00112.2007
6. Han, S. H., & Mallampalli, R. K. (2015). The role of surfactant in lung disease and host defense against pulmonary infections. *Annals of the American Thoracic Society*, *12*(5), 765–774. https://doi.org/10.1513/AnnalsATS.201411-507FR
7. Hofer, C. C., Woods, P. S., & Davis, I. C. (2015). Infection of mice with influenza A/WSN/33 (H1N1) virus alters alveolar type II cell phenotype. *American Journal of Physiology-Lung Cellular and Molecular Physiology*, *308*(7), L628–L638. https://doi.org/10.1152/ajplung.00373.2014
8. Wahid, F., Shehzad, A., Khan, T., & Kim, Y. Y. (2010). MicroRNAs: Synthesis, mechanism, function, and recent clinical trials. *Biochimica et Biophysica Acta - Molecular Cell Research*, *1803*(11), 1231–1243. https://doi.org/10.1016/j.bbamcr.2010.06.013
9. Faraoni, I., Antonetti, F. R., Cardone, J., & Bonmassar, E. (2009). miR-155 gene: A typical multifunctional microRNA. *Biochimica et Biophysica Acta - Molecular Basis of Disease*, *1792*(6), 497–505. https://doi.org/10.1016/j.bbadis.2009.02.013
10. Winter, J., Jung, S., Keller, S., Gregory, R. I., & Diederichs, S. (2009). Many roads to maturity: MicroRNA biogenesis pathways and their regulation. *Nature Cell Biology*, *11*(3), 228–234. https://doi.org/10.1038/ncb0309-228
11. Nogales, A., Baker, S. F., & Martínez-Sobrido, L. (2015). Replication-competent influenza A viruses expressing a red fluorescent protein. *Virology*, *476*, 206–216. https://doi.org/10.1016/j.virol.2014.12.006
12. Aeffner, F., Bolon, B., & Davis, I. C. (2015). Mouse models of acute respiratory distress syndrome. *Toxicologic Pathology*, *43*(8), 1074–1092. https://doi.org/10.1177/0192623315598399

13. Liu, Q., Zhou, Y. H., & Yang, Z. Q. (2016). The cytokine storm of severe influenza and development of immunomodulatory therapy. *Cellular and Molecular Immunology*, *13*(1), 3–10. https://doi.org/10.1038/cmi.2015.74
14. Fukao, T., & Koyasu, S. (2003). PI3K and negative regulation of TLR signaling. *Trends in Immunology*, *24*(7), 358–363. https://doi.org/10.1016/S1471-4906(03)00139-X
15. Mümmler, C., Burgy, O., Hermann, S., Mutze, K., Günther, A., & Königshoff, M. (2018). Cell-specific expression of runt-related transcription factor 2 contributes to pulmonary fibrosis. *FASEB Journal*, *32*(2), 703–716. https://doi.org/10.1096/fj.201700482R
16. Lee, Y., Kim, M., Han, J., Yeom, K.-H., Lee, S., Baek, S. H., & Kim, V. N. (2004). MicroRNA genes are transcribed by RNA polymerase II. *The EMBO Journal*, *23*(20), 4051–4060. https://doi.org/10.1038/sj.emboj.7600385
17. Sieweke, M. H., Tekotte, H., Frampton, J., & Graf, T. (1996). MafB is an interaction partner and repressor of Ets-1 that inhibits erythroid differentiation. *Cell*, *85*(1), 49–60. https://doi.org/10.1016/S0092-8674(00)81081-8
18. Thoompumkal, I. J., Rehna, K., Anbarasu, K., & Mahalingam, S. (2016). Leucine Zipper Down-regulated in Cancer-1 (LDOC1) interacts with Guanine nucleotide binding protein-like 3-like (GNL3L) to modulate Nuclear Factor-kappa B (NF-κB) signaling during cell proliferation. *Cell Cycle*, *15*(23), 3251–3267. https://doi.org/10.1080/15384101.2016.1242534
19. Bertin, J., Wang, L., Guo, Y., Jacobson, M. D., Poyet, J. L., Srinivasula, S. M., … Alnemri, E. S. (2001). CARD11 and CARD14 Are Novel Caspase Recruitment Domain (CARD)/Membrane-associated Guanylate Kinase (MAGUK) Family Members that Interact with BCL10 and Activate NF-κB. *Journal of Biological Chemistry*, *276*(15), 11877–11882. https://doi.org/10.1074/jbc.M010512200
20. Utani, A. (2010). Laminin ??3 chain-derived peptide promotes keratinocyte migration and wound closure: Clustering of syndecan-4 and integrin ??1. *Seikagaku*, *82*(4), 327–331. https://doi.org/10.1091/mbc.E08
21. Atlas, S. A. (2007). The Renin-Angiotensin Aldosterone System: Pathophysiological Role and Pharmacologic Inhibition. *Journal of Managed Care Pharmacy*, *13*(8 Supp B), 9–20. https://doi.org/10.18553/jmcp.2007.13.s8-b.9

IX. Supplemental Material

RT² Profiler™ PCR Array Mouse miR-155 Targets:

Position-RefSeq Number-Symbol-Description

A01 NM_177762 Aak1 AP2 associated kinase 1 A02 NM_177322 Agtr1a Angiotensin II receptor, type 1a A03 NM_009645 Aicda Activation-induced cytidine deaminase A04 NM_007462 Apc Adenomatosis polyposis coli A05 NM_175251 Arid2 AT rich interactive domain 2 (ARID, RFX-like) A06 NM_019514 Astn2 Astrotactin 2 A07 NM_007520 Bach1 BTB and CNC homology 1 A08 NM_178782 Bcorl1 BCL6 co-repressor-like 1 A09 NM_175362 Card11 Caspase recruitment domain family, member 11 A10 NM_009883 Cebpb CCAAT/enhancer binding protein (C/EBP), beta A11 NM_177224 Chd9 Chromodomain helicase DNA binding protein 9 A12 NM_134002 Csnk1g2 Casein kinase 1, gamma 2 B01 NM_010516 Cyr61 Cysteine rich protein 61 B02 NM_029585 Det1 De-etiolated homolog 1 (Arabidopsis) B03 NM_026191 Dhx40 DEAH (Asp-Glu-Ala-His) box polypeptide 40 B04 NM_010063 Dync1i1 Dynein cytoplasmic 1 intermediate chain 1 B05 NM_010104 Edn1 Endothelin 1 B06 NM_011808 Ets1 E26 avian leukemia oncogene 1, 5' domain B07 NM_010175 Fadd Fas (TNFRSF6)-associated via death domain B08 NM_008008 Fgf7 Fibroblast growth factor 7 B09 NM_019740 Foxo3 Forkhead box O3 B10 NM_011816 G3bp2 GTPase activating protein (SH3 domain) binding protein 2 B11 NM_013526 Gdf6 Growth differentiation factor 6 B12 NM_010437 Hivep2 Human immunodeficiency virus type I enhancer binding protein 2 C01 NM_198090 Hnrnpa3 Heterogeneous nuclear ribonucleoprotein A3 C02 NM_010511 Ifngr1 Interferon gamma receptor 1 C03 NM_019777 Ikbke Inhibitor of kappaB kinase epsilon C04 NM_010561 Ilf3 Interleukin enhancer binding factor 3 C05 NM_010566 Inpp5d Inositol polyphosphate-5-phosphatase D C06 NM_028679 Irak3 Interleukin-1 receptor-associated kinase 3 C07 NM_021878 Jarid2 Jumonji, AT rich interactive domain 2 C08 NM_021284 Kras V-Ki-ras2 Kirsten rat sarcoma viral oncogene homolog C09 NM_001018087 Ldoc1 Leucine zipper, down-regulated in cancer 1 C10 NM_175116 Lpar6 Lysophosphatidic acid receptor 6 C11 NM_010658 Mafb V-maf musculoaponeurotic fibrosarcoma oncogene family, protein B (avian) C12 NM_010771 Matr3 Matrin 3 D01 NM_010788 Mecp2 Methyl CpG binding protein 2 D02 NM_001033713 Mef2a Myocyte enhancer factor 2A D03 NM_010789 Meis1 Meis homeobox 1 D04 NM_026810 Mlh1 MutL homolog 1 (E. coli) D05 NM_008628 Msh2 MutS homolog 2 (E. coli) D06 NM_010830 Msh6 MutS homolog 6 (E. coli) D07 NM_010848 Myb Myeloblastosis oncogene D08 NM_019472 Myo10 Myosin X D09 NM_022996 Ndfip1 Nedd4 family interacting protein 1 D10 NM_010900 Nfatc2ip Nuclear factor of activated T-cells, cytoplasmic, calcineurin-dependent 2 interacting protein 3 Position RefSeq Number Symbol Description D11 NM_021361 Nova1 Neuro-oncological ventral antigen 1	D12 NM_013626 Pam Peptidylglycine alpha-amidating monooxygenase E01 NM_011063 Pea15a Phosphoprotein enriched in astrocytes 15A E02 NM_023324 Peli1 Pellino 1 E03 NM_172303 Jade1 PHD finger protein 17 E04 NM_176916 Pld5 Phospholipase D family, member 5 E05 NM_024457 Rap1b RAS related protein 1b E06 NM_016802 Rhoa Ras homolog gene family, member A E07 NM_009068 Ripk1 Receptor (TNFRSF)-interacting serine-threonine kinase 1 E08 NM_001177869 Rreb1 Ras responsive element binding protein 1 E09 NM_009820 Runx2 Runt related transcription factor 2 E10 NM_001127725 Sec14l5 SEC14-like 5 (S. cerevisiae) E11 NM_001009818 Sept11 Septin 11 E12 NM_011355 Spi1 SFFV proviral integration 1 F01 NM_011385 Ski Ski sarcoma viral oncogene homolog (avian) F02 NM_028151 Skiv2l2 Superkiller viralicidic activity 2-like 2 (S. cerevisiae) F03 NM_008539 Smad1 MAD homolog 1 (Drosophila) F04 NM_010754 Smad2 MAD homolog 2 (Drosophila) F05 NM_008541 Smad5 MAD homolog 5 (Drosophila) F06 NM_009896 Socs1 Suppressor of cytokine signaling 1 F07 NM_009233 Sox1 SRY-box containing gene 1 F08 NM_172675 Stx16 Syntaxin 16 F09 NM_172440 Stxbp5l Syntaxin binding protein 5-like F10 NM_138667 Tab2 TGF-beta activated kinase 1/MAP3K7 binding protein 2 F11 NM_026456 Tceb1 Transcription elongation factor B (SIII), polypeptide 1 F12 NM_011600 Tle4 Transducin-like enhancer of split 4, homolog of Drosophila E(spl) G01 NM_145375 Tm6sf1 Transmembrane 6 superfamily member 1 G02 NM_024214 Tomm20 Translocase of outer mitochondrial membrane 20 homolog (yeast) G03 NM_021897 Trp53inp1 Transformation related protein 53 inducible nuclear protein 1 G04 NM_172298 Tshz3 Teashirt zinc finger family member 3 G05 NM_027192 Ttl Tubulin tyrosine ligase G06 NM_025650 Uqcr11 Ubiquinol-cytochrome c reductase, complex III subunit XI G07 NM_021522 Usp14 Ubiquitin specific peptidase 14 G08 NM_177832 Zfp236 Zinc finger protein 236 G09 NM_001033341 Zfp407 Zinc finger protein 407 G10 NM_201609 Zfp652 Zinc finger protein 652 G11 NM_009575 Zic3 Zinc finger protein of the cerebellum 3 G12 NM_029498 Zmym2 Zinc finger, MYM-type 2 H01 NM_007393 Actb Actin, beta H02 NM_009735 B2m Beta-2 microglobulin H03 NM_008084 Gapdh Glyceraldehyde-3-phosphate dehydrogenase H04 NM_010368 Gusb Glucuronidase, beta H05 NM_008302 Hsp90ab1 Heat shock protein 90 alpha (cytosolic), class B member 1 H06 SA_00106 MGDC Mouse Genomic DNA Contamination H07 SA_00104 RTC Reverse Transcription Control H08 SA_00104 RTC Reverse Transcription Control H09 SA_00104 RTC Reverse Transcription Control H10 SA_00103 PPC Positive PCR Control H11 SA_00103 PPC Positive PCR Control H12 SA_00103 PPC Positive PCR Control